ACS MATERIALS Au
AN OPEN ACCESS JOURNAL OF THE AMERICAN CHEMICAL SOCIETY

pubs.acs.org/materialsau
Article

Cellular Senescence Program is Sensitive to Physical Differences in Polymeric Tissue Scaffolds

Parul Yadav, Rahul Shah, Anindo Roy, Sibani Jani, Kaushik Chatterjee,* and Deepak Kumar Saini*

Cite This: ACS Mater. Au 2024, 4, 35−44
Read Online

ACCESS | Metrics & More | Article Recommendations | Supporting Information

ABSTRACT: A typical cellular senescence program involves exposing cells to DNA-damaging agents such as ionization radiation or chemotherapeutic drugs, which cause multipronged changes, including increased cell size and volume, the onset of enhanced oxidative stress, and inflammation. In the present study, we examined if the senescence onset decision is sensitive to the design, porosity, and architecture of the substrate. To address this, we generated a library of polymeric scaffolds widely used in tissue engineering of varied stiffness, architecture, and porosity. Using irradiated A549 lung cancer cells, we examined the differences between cellular responses in these 3D scaffold systems and observed that senescence onset is equally diminished. When compared to the two-dimensional (2D) culture formats, there were profound changes in cell size and senescence induction in three-dimensional (3D) scaffolds. We further establish that these observed differences in the senescence state can be attributed to the altered cell spreading and cellular interactions on these substrates. This study elucidates the role of scaffold architecture in the cellular senescence program.

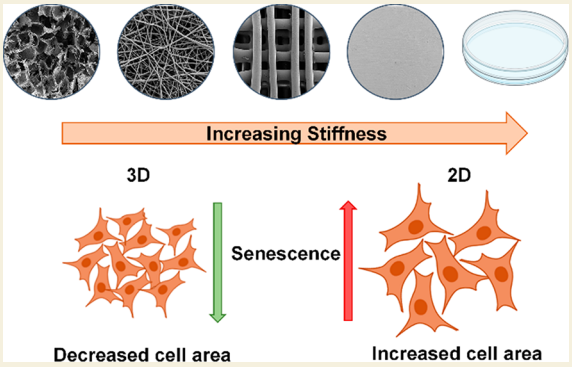

KEYWORDS: *Aging, Scaffolds, Biomaterials, Cellular Senescence, Tissue Engineering*

1. INTRODUCTION

Aging is an inevitable process leading to a progressive decline in the organism's physiology and functionality. It is driven by the accumulation of DNA damage in cells, which leads to cell cycle arrest and initiates a process called cellular senescence that leads to systemic aging if left unresolved.[1] Cellular senescence has been implicated in many age-associated ailments and is a major driver of several degenerative diseases, including cardiac and neuronal disorders, fibrosis, etc.,[2] where changes in the mechanical properties of tissues are invariably recorded. Besides, the removal of senescent cells has been shown to improve organ function in mice and human tissues.[3−6] Furthermore, several of these pathologies require interventions that utilize some form of biomaterial−cell interaction. This includes but is not limited to invasive devices, catheters,[7] pacemakers,[8] long-term biosensors,[9] and implants[10] ranging from soft polymers to hard metals. The interactions between cells and biomaterials play a critical role in modulating tissue homeostasis in the biological response to materials. It has been shown that such interactions influence cell proliferation,[11] differentiation,[12] migration,[13] immune response,[14] and survival to influence the repair or regeneration at the implanted site. For any biomaterial to perform its intended function and have good biocompatibility *in vivo*, several parameters, including its composition, surface topography,[15] mechanical properties,[16,17] and infection resistance,[18] among others,[19] are essential requirements that need to be taken into consideration. Most of the preclinical and even clinical testing of the currently available biomaterials are largely performed in young individuals where the immune system, repair, and healing capacity are efficient.[20−22,22−24] However, the regenerative capacities tend to be compromised in the geriatric population leading to delayed recovery. This difference may be attributed to the altered host response to biomaterials in aged individuals[25] which differs from that in younger individuals.

Aging is typically associated with chronic health problems, and geriatric patients are principal recipients of several biomaterial-based assistive therapies. Despite the increasing usage of biomaterials in aged patients, few studies examine the effect of aging on the host response to the material.[26] Given that senescent cells accumulate with increased age, they add another dimension to a large number of other factors which affect the biocompatibility of the introduced material. It is, therefore, imperative to investigate the interaction of senescent cells with biomaterials to engineer implants and tissue scaffolds to promote tissue regeneration in older patients.

Received: July 3, 2023
Revised: September 19, 2023
Accepted: September 22, 2023
Published: October 6, 2023

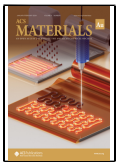

Numerous *in vitro* studies have underscored the roles of chemical, biomolecular, and physical properties of biomaterials on cell function and fate. Fibroblasts exhibit broader and flatter morphology and generate more traction force on stiffer substrates than softer ones.[27] The growth of transformed cells has been demonstrated to be supported by gelatin-coated substrates softer than 100 Pa; however, the same could not be observed in untransformed cells.[28] Surface topography such as roughness and patterning—anisotropic or isotropic, in the form of grooves, fiber, pits, pillars, etc., have been reported to markedly influence cellular fate, including for stem,[29,30] cardiac,[31] muscle,[32,33] epithelial,[34,35] and neuronal cells.[36,37] We and others have elucidated the effect of architecture on the growth, migration, and metastasis of cancer cells.[38] Other reports revealed the effect of surface patterning and stiffness on cardiac cell function[39] and osteogenic differentiation of human mesenchymal stem cells,[40] among others. The architecture of the 3D scaffold can serve as a biophysical cue to influence cell response through a combination of altered geometry and mechanical properties (stiffness).[41]

For most of these studies, the effect was recorded for proliferating cells wherein the effect is dominated by changes in the rate of cell proliferation as an outcome of the effect of the substrate changes. However, during senescence, the cells are in a state of irreversible growth arrest driven by presence of persistent DNA damage,[42] high concentration of reactive oxygen species (ROS),[43] mitochondrial dysfunction,[44] and an overall inflammatory milieu.[45,46] Effects of senescent cells and associated inflammation include the recruitment of immune cells for their clearance,[47] which disrupts normal tissue structure and function if left unresolved. Furthermore, implantation of a biomedical device/product in a geriatric patient can induce additional stress over and above the existing senescent microenvironment due to aging.[48−51] There is a limited understanding of how biomaterial properties influence the senescence status of the cells. Previously, inherent differences were reported in senescent cell behavior when cultured on soft, porous scaffolds compared to conventional two-dimensional (2D) tissue culture plates.[52] It was demonstrated that there is a fundamentally aberrant impact of culturing cells on 2D platforms, which results in the exacerbation of overall senescence signatures unlike what is recorded in 3D culturing platforms.

The goal of this work was to investigate the effect, if any, of changes in 3D scaffold architectures on the senescence state of the cells. We selected one of the most widely utilized biomaterials, polycaprolactone (PCL), which has been used in several products and devices approved for clinical use. PCL is cytocompatible, biodegradable, inexpensive, and easily processable, with excellent mechanical and degradation properties affording the fabrication of a wide range of three-dimensional (3D) substrates for hard and soft tissues. In this study, scaffolds with different architectures and stiffness (ranging from ≈8 kPa to ≈320 MPa) were fabricated from PCL such that their effect on the cellular response can be analyzed. The fabricated scaffolds were characterized for their morphology using microscopy and various physical techniques. Further, the cellular response of senescent cells was evaluated using cell morphology and gene expression profile analysis. This study can aid in designing biomaterials that reduce the adverse effects of senescent cells on an already compromised environment and provide a template framework for screening for appropriate material properties for geriatric applications.

2. MATERIALS AND METHODS

2.1. Scaffold Synthesis

2.1.1. Salt Leaching. Porous scaffolds of poly(ε-caprolactone) (PCL, average molecular weight = 80,000, Sigma-Aldrich) were fabricated by salt leaching. PCL pellets were dissolved in 2,2,2-trifluoroethanol (TFE, Spectrochem, India) at 10% (w/v) concentration. The solution was stirred continuously for 12 h for uniform mixing. Salt size ranging from 235 to 425 μm was selected as the porogen, and the solution was poured into cylindrical molds of 48 well plates. 135 μL of the solution was poured into each well containing 0.39 g of salt. The plate was dried for 24 h, and the salt was leached out in a water bath, followed by air drying. Further, the scaffolds were sterilized by exposing them to ultraviolet (UV- 254 nm) light for 1 h, followed by 70% (v/v) ethanol washes. Hereafter, these scaffolds will be referred to as SL.

2.1.2. Electrospinning. Nanofibers of PCL were fabricated by electrospinning using the ESPIN NANO V1VC instrument. 12% (w/v) feed solution was prepared by dissolving PCL pellets in TFE and stirring for 12 h. The parameters used to draw neat PCL fibers were as follows: voltage of 12 kV, a distance of 15 cm between the electrode tip and collector plate, and a flow rate of 0.5 mL/h. The fibers were collected on aluminum sheets. The nanofibrous mats were then cut into circular shapes (depending on the size of the well plate being used), washed with 70% (v/v) ethanol and sterilized by placing them under UV (254 nm) light for 1 h on each side, top, and bottom. Hereafter, the nanofibrous mats will be referred to as NF.

2.1.3. Compression Molding. Flat PCL discs were fabricated by compression molding. PCL pellets were placed in cylindrical molds of 2.5 cm diameter or 1 cm with 0.24 cm height. The PCL pellets were preheated in the mold for 30 min, followed by compression under a pressure of 2 MPa for 2 h. The fabricated discs were sterilized under UV (254 nm) light for 1 h, followed by 70% (v/v) ethanol washes. Hereafter, the fabricated PCL discs will be referred to as CM.

2.1.4. 3D Printing. 3D printed scaffolds were fabricated with a CELLINK BIO X 3D printer, using PCL pellets as the feed material. A cylindrical 3D model of 12 mm diameter and 2.5 mm height was modeled with Microsoft 3D Builder, and the structure was sliced with CELLINK Heartwave and SLIC3R software. The infill pattern and density were set to rectilinear and 45%, respectively. Printhead and print bed temperatures were set to 130 and 12 °C, respectively. The polymer was extruded with a pressure of 200 kPa, and the printhead speed was set to 3 mm/s. The printed scaffolds were sterilized under UV (254 nm) light for 1 h followed by 70% (v/v) ethanol washes. Hereafter, the 3D-printed PCL constructs will be referred to as 3DP.

2.2. Scaffold Characterization

Scanning electron microscopy (SEM) imaging was carried out using a Carl Zeiss Ultra 55 FE-SEM instrument to study the surface topography of the fabricated scaffolds. The scaffolds were gold-sputtered before imaging. The images were analyzed using ImageJ software to obtain scaffold surface parameters such as pore size, fiber diameter, interstrut distance, and diameter of struts. A universal testing machine (Instron 5967) was used for mechanical analysis of 3DP samples. Compression test was performed on cylindrical sample with 5 kN load cell and crossover speed of 1 mm/min. The compression modulus was evaluated by calculating the slope of the stress−strain curve in the linear region. The storage modulus of the nanofibers (NF) was determined by carrying out dynamic mechanical analysis (DMA) using a TA Instruments Q 800 in film tension-controlled force mode with a constant force of 3 N/min. Analysis was carried out with a rectangular-shaped sample of dimensions 15 mm × 10 mm × 0.2 mm, and the modulus was determined from the linear part of the stress−strain graph. Rectangular strips (15 mm × 5 mm × 0.5 mm) of PCL were fabricated by compression molding and used to calculate the storage modulus of PCL. A frequency sweep from 0.1 to 100 Hz was performed with the measurement at 1 Hz and a preload of 0.01 N. The same DMA instrument was used to determine the elastic modulus of the SL scaffolds in compression mode. An amplitude of 10 μm with a preload force of 0.01 N was used. All the

https://doi.org/10.1021/acsmaterialsau.3c00057
ACS Mater. Au 2024, 4, 35−44

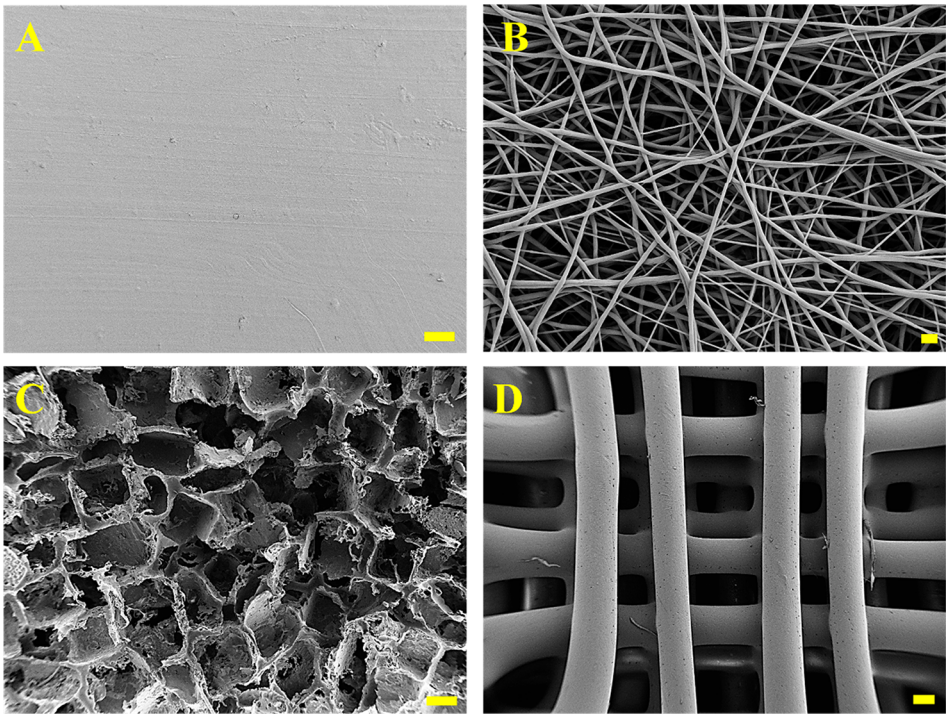

Figure 1. SEM micrographs of the various scaffolds. (A) CM disc, (B) NF mat, (C) SL scaffolds, and (D) 3DP scaffolds. Scale bar represents 200 μm in A, C, and D and 2 μm in B.

DMA measurements were performed at 37 °C. We further performed atomic force microscopy (AFM) on only salt leached scaffolds, the details of which are mentioned in the Supporting Information (SI). Differential scanning calorimetry (DSC) was also performed on all the samples (details in SI).

2.3. Cellular Studies

2.3.1. Cell Culture. The human lung epithelial carcinoma cell line, A549, was procured from ATCC. Cells were cultured in Dulbecco's minimal essential media (DMEM, Sigma) supplemented with 10% (v/v) fetal bovine serum (FBS, Gibco, Invitrogen) and 1% antibiotics-penicillin and streptomycin. Cells were cultured at 37 °C in a 5% CO_2 humidified incubator. All the scaffolds used in the study were soaked in serum-containing medium (10% FBS+DMEM) for 24 h prior to cell seeding.

2.3.2. Cellular Senescence Induction. A549 cells were exposed to 8 grays of gamma radiations (^{60}Co) using a blood irradiator, BI 2000 machine. Cells were trypsinized, the cell suspension (in DMEM) was irradiated in a 15 mL sterile polypropylene tube, and cells were immediately used for experimental seeding. Irradiated (senescent, Sen) cells and nonirradiated (nonsenescent, NS) cells were counted and seeded on tissue culture polystyrene (TCPS) dishes. Similarly, cells were seeded on different scaffolds.

2.3.3. Morphology Analysis. A549 cells, Sen and NS, were stained for F-actin and nucleus 4 days after culture in various matrices. Briefly, cells on scaffolds and 2D TCPS were fixed using 4% paraformaldehyde for 15 min, followed by permeabilization using 0.2% TritonX-100. The cells were then stained using phalloidin conjugated with Alexa Fluor 488 (Invitrogen) for 1 h at 25 °C, and DAPI (Sigma-Aldrich) was used at 1 μg/mL for 5 min at 25 °C to stain the nuclei. The samples were imaged using a laser scanning confocal microscope (Zeiss LSM 880), and the maximum intensity projections were used to calculate the cellular area using ImageJ software.

2.3.4. Senescence-Associated β-Galactosidase Activity (SAβGal). To confirm senescence in the irradiated cells, 4 days postcell seeding, both the NS and Sen cells cultured on the 2D TCPS were stained for SaβGal., as per the protocol described by Dimri et al.[53] Briefly, the cells were fixed using 0.2% (v/v) glutaraldehyde (Amresco, USA) in PBS for 15 min at room temperature. Three PBS washes were given, followed by the addition of a freshly prepared staining solution. The staining solution comprised of 1 mg mL^{-1} X-gal (GoldBio Technology, USA) in 40 mM citric acid/sodium phosphate (pH 6.0) with 150 mM NaCl, 2 mM MgCl2, 5 mM potassium ferrocyanide and 5 mM potassium ferricyanide (all chemicals from SRL, India). The cells were incubated in the staining solution overnight, washed with 1X phosphate-buffered saline (PBS) twice, and imaged using an inverted IX81 microscope equipped with a DP72 color camera (Olympus, Japan). The presence of a blue-colored stain in the cells confirmed senescence induction.

2.3.5. Senescence-Associated Markers. NS and Sen A549 cells were cultured either on 2D TCPS or scaffolds for 4 days. RNA was isolated using the RNeasy Mini Kit (Qiagen) as per the protocol described by the manufacturer. Several scaffolds were pooled for extracting RNA to obtain sufficient amounts from each scaffold system. Lysis buffer was added directly on NF, CM, and 3DP scaffolds. For SL scaffolds, each scaffold was cut into 4 smaller pieces using a scalpel, which was followed by the addition of lysis buffer. 500 ng of RNA was used to synthesize cDNA using the Verso cDNA synthesis kit (Thermofisher Scientific) according to the manufacturer's instructions. A quantitative real-time polymerase chain reaction (qRT-PCR) was performed using QIAquant 96 real-time PCR (Qiagen) using PowerUP SYBR Green Master Mix (Applied Biosystems). Gene expression was determined by calculating fold change using $2^{-\Delta\Delta ct,}$ and GAPDH was used as the housekeeping gene. The list of primers used, and their sequence is mentioned in Table S1.

2.3.6. Western Blot. NS and Sen A549 cells were cultured on 2D TCPS (60 mm Petri dish) for 4 days. We varied the cell density for Sen A549 cells from 1.5, 3, 6, and 12 x10^5 on the 60 mm Petri dish to restrict cell spreading. Since NS A549 will exhibit proliferation, these cells were seeded at 1.5 x10^5 as control. Cell lysate was prepared using Mammalian cell lysis buffer (GoldBio, USA) as per manufacturer's protocol. The total amount of protein in the lysate was estimated using Bradford's protein estimation reagent. For Western blot, 50 μg of total protein was resolved on 12% SDS-PAGE gel. This was then transferred to PVDF membrane (Merck, India) using a semidry transfer unit (Power Blotter System, Invitrogen, USA) at 25 V for 12 min. The membrane with transferred protein was blocked using Tris

https://doi.org/10.1021/acsmaterialsau.3c00057
ACS Mater. Au 2024, 4, 35−44

buffered saline with Tween 20 (TBST) buffer containing 5% BSA protein (MP Biomedicals, USA) for 1 h. The membrane was further incubated in primary antibody diluted in TBST at 4 °C overnight. Membrane was washed thrice for 10 min using TBST. This was followed by incubation with appropriate HRP tagged secondary antibody (Jackson Laboratories Inc., USA) diluted as per manufacturer's instructions and incubated for 1 h at 27 °C. Membrane was again washed thrice using TBST and subjected to chemiluminescence detection using ECL substrate (Clarity Western ECL substrate, Bio-Rad, USA). The blots were imaged in a ChemiDoc MP imaging system (Bio-Rad Inc., USA) at multiple exposure settings. The details of antibodies used have been mentioned in Table S2.

2.4. Statistical Analysis

The data were statistically analyzed by performing either one-way ANOVA or unpaired t test to evaluate the significant differences between the samples. Data are presented as mean ± standard error of the mean for $n = 3$.

3. RESULTS

To investigate the role of scaffold architecture on senescent cell behavior, PCL scaffolds with different architectures were fabricated using three techniques: salt leaching (variable pores), electrospinning (unaligned nanofibers), and 3D printing (fixed pores). TCPS, which is the conventional substrate of choice, was used as the 2D control (flat surface). Compression-molded (flat) discs of PCL sheets served as an additional 2D control to assess the differences in material composition between TCPS and PCL. The fabricated scaffolds exhibited a wide variety of topographies with varying structural parameters such as porosity and fiber diameter.

3.1. Scaffold Characterization

The topography of the fabricated scaffolds was characterized using SEM. SEM images of the compression-molded discs revealed a smooth surface (Figure 1A). SEM micrographs of the nanofibers showed the random (unaligned) arrangement of fibers deposited by electrospinning (Figure 1B), wherein the mean fiber diameter of the fibers was 585 ± 58 nm (Figure 2D). The fibers were of uniform sizes throughout the nanofibrous sheet. SEM images of the salt-leached scaffolds revealed the roughness and high porosity of the scaffold (Figure 1C). The average pore diameter was 320 ± 77 μm, with pore sizes ranging from 130 to 480 μm (Figure 2A). SEM images of the 3D printed scaffolds showed their smooth surface and uniform strut diameters and pore sizes (Figure 1D). The average strand diameter was 340 ± 23 μm (Figure 2C), and the interstrut distance was 240 ± 17 μm (Figure 2D). All scaffolds depicted porous structures with good interconnectivity which is essential for cell proliferation and survival. DSC result showed all samples to be semicrystalline (Figure S2 and Table S4).

The mechanical properties of the scaffolds were determined by UTM and DMA. The compressive modulus of the 3DP scaffolds evaluated from the stress−strain curve obtained from universal testing machine (UTM) was 54 ± 5 MPa. The storage modulus of the NF assessed from the data obtained from DMA was 1.61 ± 0.2 MPa, whereas that of SL porous scaffolds was 7.82 ± 1.5 kPa, and that of CM sheets was 315 ± 2 MPa. The 3DP ones displayed the highest stiffness of all the scaffolds, followed by NF and SL, owing to their architectural differences. Solid PCL CM discs further had high stiffness compared to other samples; however, they were still significantly lower than 2D TCPS (≈2.79 GPa). It is now very well established that 2D culture systems do not recapitulate several of the *in vivo* properties of human tissues, including architecture, stiffness, cellular interactions, matrix modeling, etc. Therefore, the scaffold systems provide us with a better mimic of the microenvironment and thus would be an appropriate/suitable alternative to conventional culture techniques.

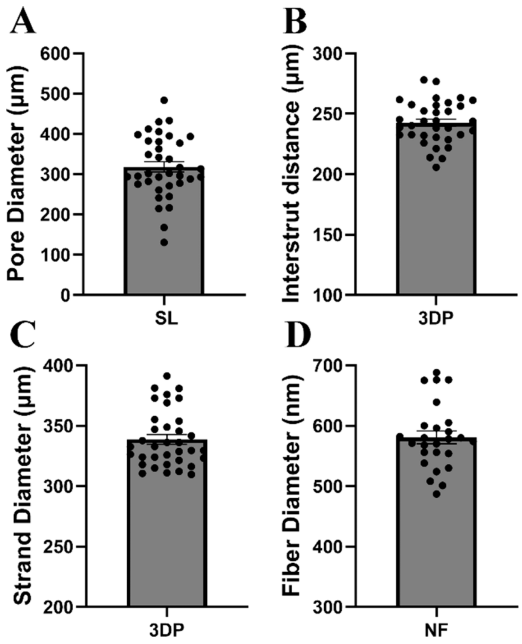

Figure 2. Quantification of scaffold parameters. (A) SL pore diameter, (B) interstrut distance in 3DP, (C) strand diameter of 3DP, and (D) NF fiber diameter. Error bars indicate the standard error of the mean.

3.2. Ionization Radiation-Based Cellular Senescence Induction

To optimize senescence induction by irradiation in A549 cells, a preliminary analysis was done by comparing the cell size of NS A549 cells with those of Sen A549 cells on 2D TCPS using ImageJ. Bright-field microscopic images of NS and Sen A549 cells are presented in Figure 3A and B, respectively. On average, the NS samples had an area of 1513 ± 82 μm^2 and a perimeter of 164 ± 14 μm, whereas the Sen cells had an area of 7737 ± 70 μm^2 and a perimeter of 358 ± 14 μm (Figure S1), implying a significant increase in cellular area and spreading. These trends corroborate the observation in the literature where the senescent cells are characterized by their larger size in 2D culture. To further verify senescence induction, samples were stained for SAβGal activity, which is known to be higher in the Sen cells compared to the NS cells[53] (Figure 3D and E). NS showed, on average, 21% staining, whereas Sen exhibited 78% staining (Figure 3F). Moreover, the Sen cells exhibited increased expression of known markers, cell-cycle inhibitor p21, and senescence-associated inflammatory markers IL-6 and IL-8, as compared to NS, confirming the senescent state of the A549 cells postirradiation (Figure 3G−I).

3.3. Effect of Substrate Architecture on Cell Morphology

The effect of the scaffold architecture was studied by staining the cells for F-actin and nucleus. Figure 4 shows the cellular distribution and morphology of each type of scaffold. We observed that the Sen A549 cells on all the culture platforms had a significantly higher area than their NS counterpart corroborating well-established trends on planar 2D substrates.

https://doi.org/10.1021/acsmaterialsau.3c00057
ACS Mater. Au 2024, 4, 35−44

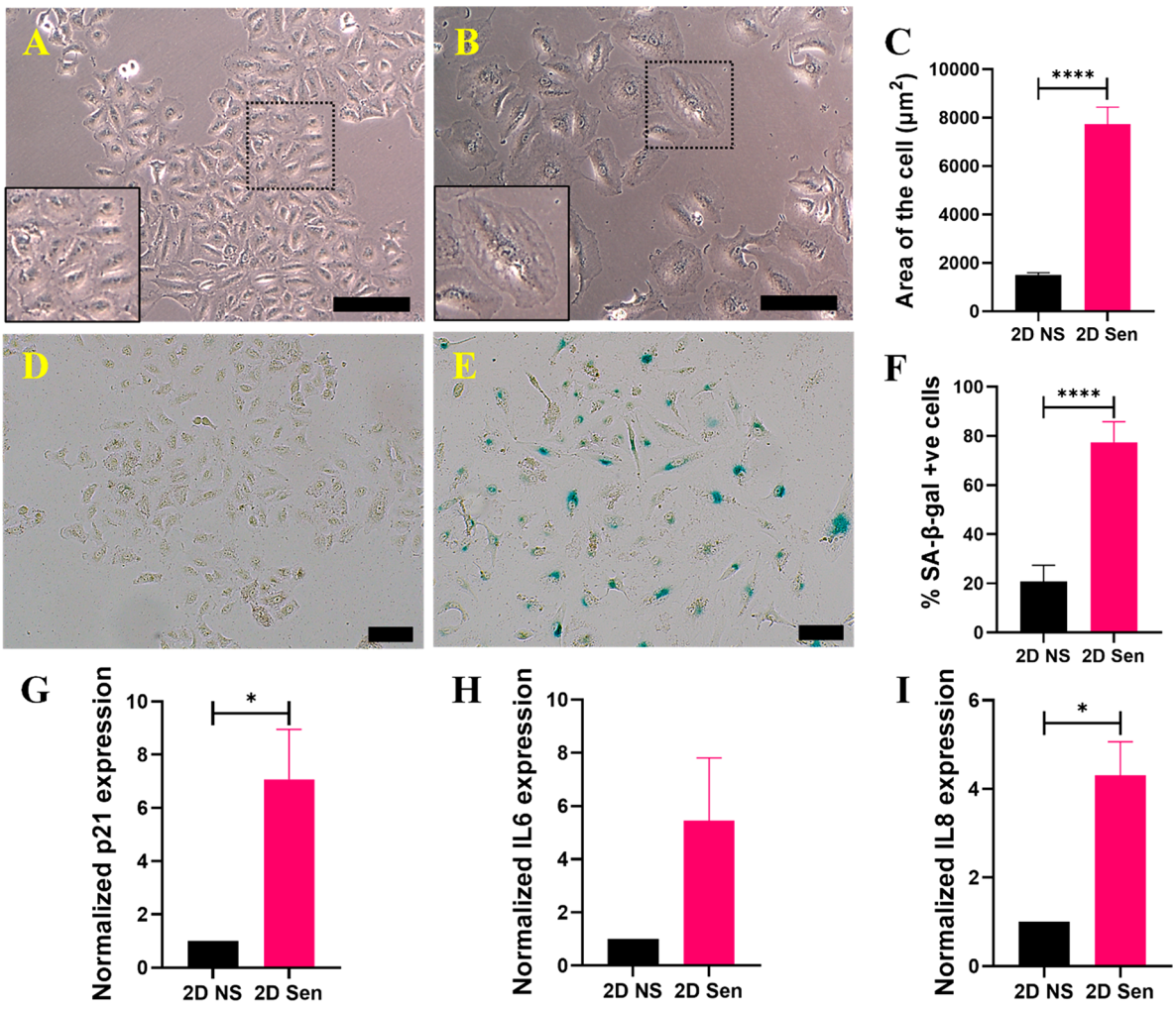

Figure 3. Assessment of senescence induction in A549 cells. Bright-field images of (A) NS and (B) Sen A549 cells (scale bar represents 80 μm). Quantification of area (C) of the cells. SaβGal staining of (D) NS and (E) Sen cells and quantification of the percentage of positively stained cells (F) (scale bar represents 100 μm). Gene expression analysis of (G) p21, (H) IL6, and (I) IL8. Error bars indicate the standard error of the mean. An unpaired t test was performed. **** indicates $p < 0.0001$, and * indicates $p < 0.05$.

Interestingly, NS cells on NF, SL, and 3DP scaffolds had a lesser area than 550 μm^2; however, cells on CM discs had an area of 1267 μm^2 (≈2.3 times higher), suggesting that the substrate architecture does play a role in determining the cellular shape and spread. When irradiated cells were allowed to become senescent on these platforms, we observed that Sen cells on CM displayed the highest cell spreading (≈5000 μm^2) among the fabricated substrates. All the other scaffolds had a cellular area lesser than 1500 μm^2. On the TCPS control (Figure 4I), we found that the NS cells measured ≈1500 μm^2, whereas the Sen cell population averaged around ≈7700 μm^2. These trends suggest that the Sen cells cultured on 3D scaffolds measure (<1500 μm^2) nearly equal to those of NS cells (≈1500 μm^2) on the 2D (TCPS and CM). This important observation indicates that the enlargement or spreading of senescent cells (widely recognized as a marker of senescence induction *in vitro*) is indeed a culture-induced (2D format) artifact and that this could possibly be a reason for elevated senescence signatures on TCPS that have been reported to date in the literature. We have reported a similar observation wherein irradiated HeLa cells cultured on soft, porous PCL scaffolds had lower cell area and subdued senescence signatures than TCPS.[52] Cell size can vary a hundred folds in humans, ranging from red blood cells[54] (≈8 μm) to neurons (≈100 μm). However, within each cell type, there is a tight regulation of standard size with little deviation. Cell spread area has been shown to be correlated with several important cell functionalities, and deviation from this has been shown to slow down cell processes. The work of Neurohr et al. showed that, with increasing cell size, the cell could not meet the demand of synthesizing enough proteins to maintain normal cell functions.[55] This results in dilution of the cytoplasm and disruption of cell division. With cellular DNA already damaged during senescence, it leads to disruption of the surface area to volume ratio, resulting in overall functional decline. The 3D scaffold systems used in this study partially restrict this phenomenon, thereby indirectly reducing the detrimental effects or the extent of damage to Sen cells. Notably, Sen cells were well spread on both 2D formats (TCPS and CM), indicating that the architecture is dominant over differences in material composition and/or hydrophobicity. The putative differences in composition, wettability, and possibly minor differences in surface roughness seem to have induced only modest differences in cell spreading. We propose that the design of a biomedical device must account for the differences in the cellular response to biomaterials by

https://doi.org/10.1021/acsmaterialsau.3c00057
ACS Mater. Au 2024, 4, 35−44

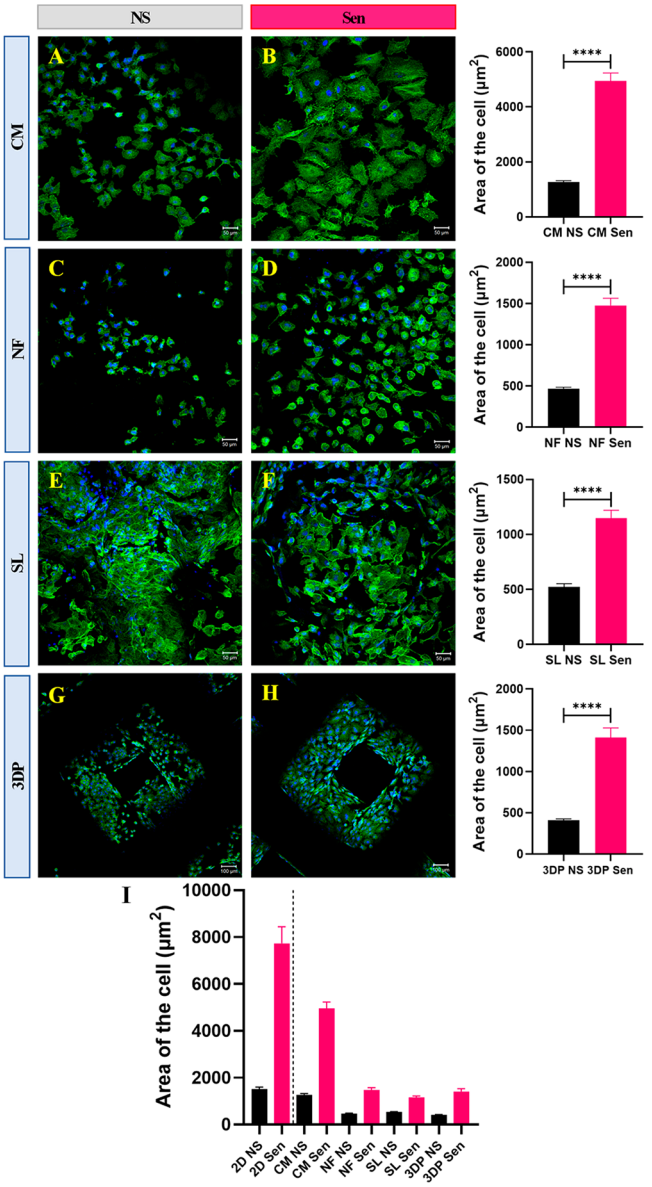

Figure 4. Cell distribution and spread on the scaffolds. (A–H) NS and Sen A549 cells were stained for F-actin (green) and nucleus (blue) with the corresponding quantification of the cellular area on each scaffold. An unpaired *t* test was performed. **** indicates $p < 0.0001$. Error bars indicate the standard error of the mean. (I) Comparative analysis of the cellular area of the culture platforms. Error bars indicate the standard error of the mean. Detailed statistical analysis of each group is shown in Table S3 of the SI.

careful design to prevent further damage and distress to an existing senescent milieu/microenvironment.

3.4. Senescence and Inflammation Status of Senescent Cells on Scaffolds

Cells actively respond to their surrounding environment, which includes both the chemical and physical environment they reside in and modulate their behavior accordingly. It is now established that substrate stiffness plays a vital role in this process and can lead to different outcomes of cellular physiology. When senescent cells were cultured on the various scaffolds, we found that despite upregulation of p21, in response to the DNA damage the cells were subjected to, the levels were consistently lower than the Sen cells on 2D TCPS (Figure 5A). Inflammation was present in all the scaffold systems as senescent cells are known to maintain slow chronic inflammatory status.[51]

Among the scaffold systems, SL and 3DP exhibited the lowest upregulation in senescence pathway induction (p21). Cells on CM had the highest levels of p21 expression since the stiffness of the substrate was high with no structural variations. In comparison, 3DP scaffolds with relatively lower stiffness but porous architecture depicted lower induction of p21, implying that architecture contributes to the cellular response. Softer scaffolds, SL and NF, each displayed lower inflammatory status too. Several studies have highlighted the importance of stiffness in regulating senescence via cytoskeletal changes (mechanotransduction), and that could be a plausible reason for the effects seen in these various scaffolds. Further, pore size (architecture) is also reported to alter cellular function. Since several factors can modulate cellular response, we envision that the effect we see in the NS and Sen cells on different structural modalities is a multifactorial outcome. Since the cellular area on scaffolds had decreased markedly, we hypothesized if cell spreading (and thereby cell area) plays a role in senescence induction. We performed a simple experiment of restricting cellular spread by seeding Sen A549 on a 60 mm Petri dish and varying cell seeding density by seeding at 1.5, 3, 6, or 12 ($\times 10^5$) cells/dish. This allowed for abundant spread area in the lowest cell density to crowding and thus restricted spreading for the highest cell density. We then probed p21 protein levels by Western blotting and found that the available cell spread area has a direct effect on senescence induction. The lower cell densities (1.5 and 3×10^5) demonstrated upregulation of p21 whereas the higher cell densities (6 and 12×10^5) showed a decrease (Figure 5B). This again reiterates the fact that cell size is a crucial determinant of cellular functionality. The aberrant increase in cell size during senescence seen *in vitro* is a culture artifact and thereby the effects seen are misrepresentation of the *in vivo* mechanisms. 3D scaffolds help minimize these effects and offer important design parameters for engineering tissue scaffolds for regeneration *in vivo* and better biomimetic *in vitro* model systems. This study demonstrates that culture substrate plays an important role in senescence induction program.

4. DISCUSSION

Aging is a significant contributor to several pathologies and is the greatest risk factor for most chronic diseases,[56] and cellular senescence is a major contributing factor to this.[57−61] Senescence is a stress response to numerous distinct stimuli leading to the progressive deterioration of cellular functions at multiple levels. It is essentially an irreversible growth-arrested state when cells are exposed to a high but sublethal dose of DNA damage.[1] Senescent cells are characterized by stable cell cycle arrest,[62,63] altered gene expression, resistance to apoptosis, chromatin reorganization[64−66] as well as morphological and metabolic changes.[67] *In vitro*, these cells have a larger and flatter body as compared to healthy cells with enhanced actin stress fibers.[55,68] They are also characterized by large nuclei, multinuclei, and chromatin reorganization and are relatively more granulated than their nonsenescent counterpart.[69−71] Several of the age -associated diseases require treatments in the form of replacement, support, or intervention using some form of biomaterials. It could range from the insertion of pacemakers,[72] stents, plates, screws,[73] etc., to breast implants,[74] catheters,[75] dental implants,[10] and even

https://doi.org/10.1021/acsmaterialsau.3c00057
ACS Mater. Au 2024, 4, 35−44

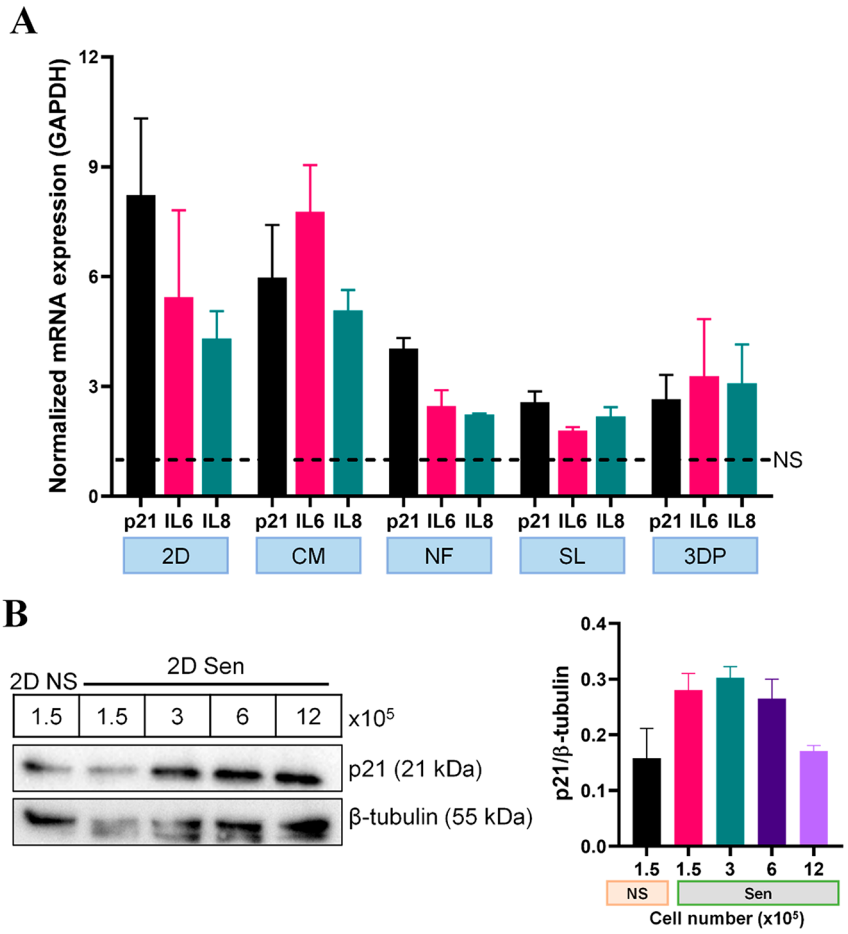

Figure 5. Senescence and inflammation-associated gene expression analysis. (A) Gene expression analysis of p21, IL6, and IL8 in NS and Sen A549 cells cultured on various scaffold systems. Dotted line represents NS of individual scaffold (which has been normalized to 1). Error bars indicate the standard error of the mean. (B) Protein levels of p21 analyzed through Western blotting and quantification.

contact lenses.[76] With the decline in overall functionality and regenerative capabilities of geriatric populations, the success rates of biomaterials also fall.[77] Thus, investigating the interactions between aged tissue/cells and biomaterials remains essential. Understanding the response of aged cells to different topological cues and structures needs to be evaluated when developing materials that directly interact with aged cells for applications, as both topical and interventional forms of biomaterials lead to foreign body reactions which act as an added stress on an already existing inflammatory microenvironment.[78,79]

This study examined the effect, if any, of the 3D scaffold architecture on the senescent cells. We recorded that substrate properties affected the cell morphology of the A549 cells and scaffold stiffness varied from kPa to MPa compared to 2D TCPS (GPa). For a given material, i.e, PCL, we varied the structural properties of the scaffolds resulting in various pore sizes, stiffness, and architecture. These led to significant changes in cellular morphology and arrangement, thereby modulating senescence signatures. The cellular area between scaffolds did not vary much in between 3D, but there was a significant difference between NS and Sen cell populations. On CM discs, NS cell areas are similar to those of Sen cells in the scaffolds. Compared to the 2D TCPS, there was no difference between the NS cell area of CM; however, a lower stiffness of CM did render a decreased area in the Sen cell population. This suggests that stiffness is an essential parameter in modulating cellular properties. When variation in pores and geometry was introduced, there was little difference between the fabricated scaffolds. We observed that all PCL substrates (2D and 3D) were semicrystalline. Though there were some differences in the degree of degree of crystallinity, there were no clear trends correlating it with the senescence markers, which further indicates that differences in architecture primarily affected the cell response.

Studies have shown that pore diameter and geometry affect the alignment of cells and, ultimately, the structure of the desired tissue.[80] Different studies have shown that higher cell viability and proliferation are associated with porous biomaterials with bigger pores, which can be related to better diffusion of nutrients and gases in the interior region of these structures.[81] Nanoscale topographies are also known to elicit diverse cell behavior, ranging from cell adhesion, orientation, motility, and cytoskeletal changes, and modulate intracellular signaling pathways.[82] The type of topography, such as fibers, ridges, pillars, grooves, and pits, and their symmetry, e.g., aligned, random, or orthogonal, have also been reported to modulate cell behavior.[15] In a study by Kumar et al., it was demonstrated that human bone marrow stromal cells expressed unique gene expression signatures depending on the type of scaffold structure.[83] Scaffolds with nanofibers could drive these cells to osteogenic lineage without additional supplements. In our study, all the scaffolds depicted an increase in the cell cycle inhibition gene, p21; however, the levels were lower than those

https://doi.org/10.1021/acsmaterialsau.3c00057
ACS Mater. Au 2024, 4, 35−44

for 2D TCPS. The presence of an inflammatory milieu was evident in all the cultural systems. This implies that senescent cells respond to the inherent material property rather than architecture in macro-sized scaffold systems. This study further strengthens the fact that biological processes vary significantly between substrates, and there is a need to investigate aging/senescence on more platforms. Since the cellular response depends on multiple components such as substrate stiffness, architecture, pore size, presence of fibers, alignment, etc., we believe that several/combinations of these are involved in invoking a specific outcome. We also established that cell morphology plays an important role in determining biological response.[84] However, additional studies will be necessary to design effective implants, materials, and tissue engineering scaffolds to meet the need of an increasingly aged population.

5. CONCLUSION

We prepared a library of culture platforms using PCL to test differences in the cellular senescence induction program. This was achieved by varying the 3D scaffold stiffness and porosity and comparing it with the conventional culture method of 2D culture dishes and 2D substrates of PCL. We observed that while there were subtle differences between the different 3D scaffold systems, marked alterations were found in comparison with 2D substrates. We attributed these differences to changes in cell size which leads to changes in cellular functionality. This study highlights the role of cellular size, substrate architecture, and stiffness in regulating cellular senescence. Further, these 3D scaffolds can be utilized for testing of drugs to eliminate senescent cells such as senolytics and senostatics, as they mimic the *in vivo* tissue architecture more closely than 2D culture plates.

■ ASSOCIATED CONTENT

Supporting Information

The Supporting Information is available free of charge at https://pubs.acs.org/doi/10.1021/acsmaterialsau.3c00057.

> Comparative analysis of the cell perimeter on various scaffolds, details of primers and antibodies used, detailed statistical analysis for Figure 4I, AFM measurement, DSC measurements and complete blot image for Western blotting (PDF)

■ AUTHOR INFORMATION

Corresponding Authors

Kaushik Chatterjee − *Department of Bioengineering and Department of Materials Engineering, Indian Institute of Science, Bangalore, India 560012;* orcid.org/0000-0002-7204-2926; Email: kchatterjee@iisc.ac.in

Deepak Kumar Saini − *Department of Bioengineering, Indian Institute of Science, Bangalore, India 560012; Department of Developmental Biology and Genetics, C.V Raman Avenue, Indian Institute of Science, Bangalore, India 560012;* orcid.org/0000-0001-6671-7256; Email: deepaksaini@iisc.ac.in

Authors

Parul Yadav − *Department of Bioengineering, Indian Institute of Science, Bangalore, India 560012;* orcid.org/0000-0002-6257-7783

Rahul Shah − *Department of Materials Engineering, Indian Institute of Science, Bangalore, India 560012*

Anindo Roy − *Department of Materials Engineering, Indian Institute of Science, Bangalore, India 560012;* orcid.org/0000-0001-7307-3436

Sibani Jani − *Department of Bioengineering, Indian Institute of Science, Bangalore, India 560012*

Complete contact information is available at: https://pubs.acs.org/10.1021/acsmaterialsau.3c00057

Author Contributions

CRediT: **Parul Yadav** conceptualization, data curation, formal analysis, writing-original draft; **Rahul Shah** conceptualization, data curation, formal analysis, writing-original draft; **Anindo Roy** data curation, formal analysis, writing-review & editing; **Sibani Jani** data curation, formal analysis; **Kaushik Chatterjee** conceptualization, funding acquisition, project administration, supervision, writing-review & editing; **Deepak Kumar Saini** conceptualization, project administration, supervision, writing-review & editing.

Notes

The authors declare no competing financial interest.

■ ACKNOWLEDGMENTS

The authors acknowledge support from the Science and Engineering Research Board (SERB), Government of India (IPA/2020/000025). The authors acknowledge the central imaging facility of the Division of Biological Sciences and the mechanical testing facility at CeNSE. Authors also thank Dr. Sagar Nilawar for his help with DMA.

■ REFERENCES

(1) Jeyapalan, J. C.; Sedivy, J. M. Cellular Senescence and Organismal Aging. *Mech Ageing Dev* **2008**, *129* (7−8), 467−474.

(2) Childs, B. G.; Durik, M.; Baker, D. J.; van Deursen, J. M. Cellular Senescence in Aging and Age-Related Disease: From Mechanisms to Therapy. *Nat. Med.* **2015**, *21* (12), 1424−1435.

(3) Xu, M.; Pirtskhalava, T.; Farr, J. N.; Weigand, B. M.; Palmer, A. K.; Weivoda, M. M.; Inman, C. L.; Ogrodnik, M. B.; Hachfeld, C. M.; Fraser, D. G.; Onken, J. L.; Johnson, K. O.; Verzosa, G. C.; Langhi, L. G. P.; Weigl, M.; Giorgadze, N.; LeBrasseur, N. K.; Miller, J. D.; Jurk, D.; Singh, R. J.; Allison, D. B.; Ejima, K.; Hubbard, G. B.; Ikeno, Y.; Cubro, H.; Garovic, V. D.; Hou, X.; Weroha, S.; Robbins, P. D.; Niedernhofer, L. J.; Khosla, S.; Tchkonia, T.; Kirkland, J. L. Senolytics Improve Physical Function and Increase Lifespan in Old Age. *Nat. Med.* **2018**, *24* (8), 1246−1256.

(4) Cai, Y.; Zhou, H.; Zhu, Y.; Sun, Q.; Ji, Y.; Xue, A.; Wang, Y.; Chen, W.; Yu, X.; Wang, L.; Chen, H.; Li, C.; Luo, T.; Deng, H. Elimination of Senescent Cells by β-Galactosidase-Targeted Prodrug Attenuates Inflammation and Restores Physical Function in Aged Mice. *Cell Res.* **2020**, *30* (7), 574−589.

(5) Schafer, M. J.; White, T. A.; Iijima, K.; Haak, A. J.; Ligresti, G.; Atkinson, E. J.; Oberg, A. L.; Birch, J.; Salmonowicz, H.; Zhu, Y.; Mazula, D. L.; Brooks, R. W.; Fuhrmann-Stroissnigg, H.; Pirtskhalava, T.; Prakash, Y. S.; Tchkonia, T.; Robbins, P. D.; Aubry, M. C.; Passos, J. F.; Kirkland, J. L.; Tschumperlin, D. J.; Kita, H.; LeBrasseur, N. K. Cellular Senescence Mediates Fibrotic Pulmonary Disease. *Nat. Commun.* **2017**, *8* (1), 14532.

(6) Lewis-McDougall, F. C.; Ruchaya, P. J.; Domenjo-Vila, E.; Shin Teoh, T.; Prata, L.; Cottle, B. J.; Clark, J. E.; Punjabi, P. P.; Awad, W.; Torella, D.; Tchkonia, T.; Kirkland, J. L.; Ellison-Hughes, G. M. Aged-senescent Cells Contribute to Impaired Heart Regeneration. *Aging Cell* **2019**, *18* (3), No. e12931.

(7) Beiko, D. T.; Knudsen, B. E.; Watterson, J. D.; Denstedt, J. D. Biomaterials in Urology. *Curr. Urol Rep* **2003**, *4* (1), 51−55.
(8) Ebert, M. J.; Lyu, S.-P..; Rise, M. T.; Wolf, M. F. 4 - Biomaterials for Pacemakers, Defibrillators and Neurostimulators. In *Biomaterials for Artificial Organs*; Lysaght, M., Webster, T. J., Eds.; Woodhead Publishing Series in Biomaterials; Woodhead Publishing, 2011; pp 81−112. DOI: 10.1533/9780857090843.1.81.
(9) *Biomaterials and Biopolymers for the Development of Biosensors*; Springer: Singapore, 2023. https://link.springer.com/chapter/10.1007/978-981-19-8501-0_1 (accessed 2023-06-22).
(10) Saini, M.; Singh, Y.; Arora, P.; Arora, V.; Jain, K. Implant Biomaterials: A Comprehensive Review. *World J. Clin Cases* **2015**, *3* (1), 52−57.
(11) Mohamed, D. A.; Abdelfattah, M. I.; Aboulezz, E. H. A. The Effect of Three Different Biomaterials on Proliferation and Viability of Human Dental Pulp Stem Cells (In-Vitro Study). *Open Access Maced J. Med. Sci.* **2017**, *5* (5), 657−663.
(12) Jang, H.-K.; Kim, B.-S. Modulation of Stem Cell Differentiation with Biomaterials. *Int. J. Stem Cells* **2010**, *3* (2), 80−84.
(13) Harley, B. A. C.; Kim, H.-D.; Zaman, M. H.; Yannas, I. V.; Lauffenburger, D. A.; Gibson, L. J. Microarchitecture of Three-Dimensional Scaffolds Influences Cell Migration Behavior via Junction Interactions. *Biophys. J.* **2008**, *95* (8), 4013−4024.
(14) Antmen, E.; Vrana, N. E.; Hasirci, V. The Role of Biomaterials and Scaffolds in Immune Responses in Regenerative Medicine: Macrophage Phenotype Modulation by Biomaterial Properties and Scaffold Architectures. *Biomater. Sci.* **2021**, *9* (24), 8090−8110.
(15) Metavarayuth, K.; Sitasuwan, P.; Zhao, X.; Lin, Y.; Wang, Q. Influence of Surface Topographical Cues on the Differentiation of Mesenchymal Stem Cells in Vitro. *ACS Biomater Sci. Eng.* **2016**, *2* (2), 142−151.
(16) Wells, R. G. The Role of Matrix Stiffness in Regulating Cell Behavior. *Hepatology* **2008**, *47* (4), 1394−1400.
(17) Janmey, P. A.; Fletcher, D. A.; Reinhart-King, C. A. Stiffness Sensing by Cells. *Physiol. Rev.* **2020**, *100* (2), 695−724.
(18) Campoccia, D.; Montanaro, L.; Arciola, C. R. A Review of the Biomaterials Technologies for Infection-Resistant Surfaces. *Biomaterials* **2013**, *34* (34), 8533−8554.
(19) Tang, L.; Thevenot, P.; Hu, W. Surface Chemistry Influences Implant Biocompatibility. *Current Topics in Medicinal Chemistry* **2008**, *8* (4), 270−280.
(20) Xu, J.; Nie, N.; Wu, B.; Li, Y.; Gong, L.; Yao, X.; Zou, X.; Ouyang, H. The Personalized Application of Biomaterials Based on Age and Sexuality Specific Immune Responses. *Biomaterials* **2021**, *278*, 121177.
(21) Herrera, A. P.; Snipes, S. A.; King, D. W.; Torres-Vigil, I.; Goldberg, D. S.; Weinberg, A. D. Disparate Inclusion of Older Adults in Clinical Trials: Priorities and Opportunities for Policy and Practice Change. *Am. J. Public Health* **2010**, *100* (Suppl 1), S105−S112.
(22) Shenoy, P.; Harugeri, A. Elderly Patients' Participation in Clinical Trials. *Perspect Clin Res.* **2015**, *6* (4), 184−189.
(23) Sharma, A. A.; Karekar, S. R.; Shetty, Y. C. An Audit of Clinical Studies Involving Elderly Population Registered in Clinical Trials Registry of India. *J. Midlife Health* **2021**, *12* (1), 61−65.
(24) Le Saux, O.; Falandry, C. Is There an Age Threshold for Holding Off on Testing Novel Therapies? *Curr. Oncol Rep* **2018**, *20* (1), 6.
(25) Plewa, M. C. Altered Host Response and Special Infections in the Elderly. *Emerg Med. Clin North Am.* **1990**, *8* (2), 193−206.
(26) Zulman, D. M.; Sussman, J. B.; Chen, X.; Cigolle, C. T.; Blaum, C. S.; Hayward, R. A. Examining the Evidence: A Systematic Review of the Inclusion and Analysis of Older Adults in Randomized Controlled Trials. *J. Gen Intern Med.* **2011**, *26* (7), 783−790.
(27) Lo, C.-M.; Wang, H.-B.; Dembo, M.; Wang, Y. Cell Movement Is Guided by the Rigidity of the Substrate. *Biophys. J.* **2000**, *79* (1), 144−152.
(28) Wang, H.-B.; Dembo, M.; Wang, Y.-L. Substrate Flexibility Regulates Growth and Apoptosis of Normal but Not Transformed Cells. *American Journal of Physiology-Cell Physiology* **2000**, *279* (5), C1345−C1350.
(29) Krishna, L.; Dhamodaran, K.; Jayadev, C.; Chatterjee, K.; Shetty, R.; Khora, S. S.; Das, D. Nanostructured Scaffold as a Determinant of Stem Cell Fate. *Stem Cell Research & Therapy* **2016**, *7* (1), 188.
(30) Abagnale, G.; Steger, M.; Nguyen, V. H.; Hersch, N.; Sechi, A.; Joussen, S.; Denecke, B.; Merkel, R.; Hoffmann, B.; Dreser, A.; Schnakenberg, U.; Gillner, A.; Wagner, W. Surface Topography Enhances Differentiation of Mesenchymal Stem Cells towards Osteogenic and Adipogenic Lineages. *Biomaterials* **2015**, *61*, 316−326.
(31) Ghosh, L. D.; Jain, A.; Sundaresan, N. R.; Chatterjee, K. Elucidating Molecular Events Underlying Topography Mediated Cardiomyogenesis of Stem Cells on 3D Nanofibrous Scaffolds. *Materials Science and Engineering: C* **2018**, *88*, 104−114.
(32) Jain, A.; Behera, M.; Ravi, V.; Mishra, S.; Sundaresan, N. R.; Chatterjee, K. Recapitulating Pathophysiology of Skeletal Muscle Diseases in Vitro Using Primary Mouse Myoblasts on a Nanofibrous Platform. *Nanomedicine: Nanotechnology, Biology and Medicine* **2021**, *32*, 102341.
(33) Almonacid Suarez, A. M.; Zhou, Q.; van Rijn, P.; Harmsen, M. C. Directional Topography Gradients Drive Optimum Alignment and Differentiation of Human Myoblasts. *Journal of Tissue Engineering and Regenerative Medicine* **2019**, *13* (12), 2234−2245.
(34) Krishna, L.; Nilawar, S.; Ponnalagu, M.; Subramani, M.; Jayadev, C.; Shetty, R.; Chatterjee, K.; Das, D. Fiber Diameter Differentially Regulates Function of Retinal Pigment and Corneal Epithelial Cells on Nanofibrous Tissue Scaffolds. *ACS Appl. Bio Mater.* **2020**, *3* (2), 823−837.
(35) Kim, M.-H.; Sawada, Y.; Taya, M.; Kino-oka, M. Influence of Surface Topography on the Human Epithelial Cell Response to Micropatterned Substrates with Convex and Concave Architectures. *Journal of Biological Engineering* **2014**, *8* (1), 13.
(36) Liu, F.; Xu, J.; Wu, L.; Zheng, T.; Han, Q.; Liang, Y.; Zhang, L.; Li, G.; Yang, Y. The Influence of the Surface Topographical Cues of Biomaterials on Nerve Cells in Peripheral Nerve Regeneration: A Review. *Stem Cells Int.* **2021**, *2021*, 8124444.
(37) Hoffman-Kim, D.; Mitchel, J. A.; Bellamkonda, R. V. Topography, Cell Response, and Nerve Regeneration. *Annu. Rev. Biomed Eng.* **2010**, *12*, 203−231.
(38) Balachander, G. M.; Balaji, S. A.; Rangarajan, A.; Chatterjee, K. Enhanced Metastatic Potential in a 3D Tissue Scaffold toward a Comprehensive in Vitro Model for Breast Cancer Metastasis. *ACS Appl. Mater. Interfaces* **2015**, *7* (50), 27810−27822.
(39) Jain, A.; Hasan, J.; Desingu, P. A.; Sundaresan, N. R.; Chatterjee, K. Engineering an in Vitro Organotypic Model for Studying Cardiac Hypertrophy. *Colloids Surf., B* **2018**, *165*, 355−362.
(40) Meka, S. R. K.; Jain, S.; Chatterjee, K. Strontium Eluting Nanofibers Augment Stem Cell Osteogenesis for Bone Tissue Regeneration. *Colloids Surf., B* **2016**, *146*, 649−656.
(41) Yeung, T.; Georges, P. C.; Flanagan, L. A.; Marg, B.; Ortiz, M.; Funaki, M.; Zahir, N.; Ming, W.; Weaver, V.; Janmey, P. A. Effects of Substrate Stiffness on Cell Morphology, Cytoskeletal Structure, and Adhesion. *Cell Motil Cytoskeleton* **2005**, *60* (1), 24−34.
(42) d'Adda di Fagagna, F. Living on a Break: Cellular Senescence as a DNA-Damage Response. *Nat. Rev. Cancer* **2008**, *8* (7), 512−522.
(43) Davalli, P.; Mitic, T.; Caporali, A.; Lauriola, A.; D'Arca, D. ROS, Cell Senescence, and Novel Molecular Mechanisms in Aging and Age-Related Diseases. *Oxid Med. Cell Longev* **2016**, *2016*, 3565127.
(44) Martini, H.; Passos, J. F. Cellular Senescence: All Roads Lead to Mitochondria. *FEBS Journal* **2023**, *290* (5), 1186−1202.
(45) Coppé, J.-P.; Desprez, P.-Y.; Krtolica, A.; Campisi, J. The Senescence-Associated Secretory Phenotype: The Dark Side of Tumor Suppression. *Annu. Rev. Pathol* **2010**, *5*, 99−118.
(46) Nair, R. R.; Madiwale, S. V.; Saini, D. K. Clampdown of Inflammation in Aging and Anticancer Therapies by Limiting

Upregulation and Activation of GPCR, CXCR4. *npj Aging Mech Dis* **2018**, *4* (1), 1−11.
(47) Prata, L. G. P. L.; Ovsyannikova, I. G.; Tchkonia, T.; Kirkland, J. L. Senescent Cell Clearance by the Immune System: Emerging Therapeutic Opportunities. *Semin Immunol* **2018**, *40*, 101275.
(48) Carnicer-Lombarte, A.; Chen, S.-T.; Malliaras, G. G.; Barone, D. G. Foreign Body Reaction to Implanted Biomaterials and Its Impact in Nerve Neuroprosthetics. *Frontiers in Bioengineering and Biotechnology* **2021**, *9*, 622524.
(49) Dimarakis, I.; Rehman, S. M.; Asimakopoulos, G. 1 - Tissue Responses to Implanted Materials. In *Biomaterials and Devices for the Circulatory System*; Gourlay, T., Black, R. A., Eds.; Woodhead Publishing Series in Biomaterials; Woodhead Publishing, 2010; pp 3−23. DOI: 10.1533/9780857090553.1.3.
(50) Velnar, T.; Bunc, G.; Klobucar, R.; Gradisnik, L. Biomaterials and Host versus Graft Response: A Short Review. *Bosn J. Basic Med. Sci.* **2015**, *16* (2), 82−90.
(51) Sanada, F.; Taniyama, Y.; Muratsu, J.; Otsu, R.; Shimizu, H.; Rakugi, H.; Morishita, R. Source of Chronic Inflammation in Aging. *Frontiers in Cardiovascular Medicine* **2018**, *5*, 12.
(52) Yadav, P.; Chatterjee, K.; Saini, D. K. Senescent Cells in 3D Culture Show Suppressed Senescence Signatures. *Biomater. Sci.* **2021**, *9* (19), 6461−6473.
(53) Dimri, G. P.; Lee, X.; Basile, G.; Acosta, M.; Scott, G.; Roskelley, C.; Medrano, E. E.; Linskens, M.; Rubelj, I.; Pereira-Smith, O. A Biomarker That Identifies Senescent Human Cells in Culture and in Aging Skin in Vivo. *Proc. Natl. Acad. Sci. U. S. A.* **1995**, *92* (20), 9363−9367.
(54) Diez-Silva, M.; Dao, M.; Han, J.; Lim, C.-T.; Suresh, S. Shape and Biomechanical Characteristics of Human Red Blood Cells in Health and Disease. *MRS Bull.* **2010**, *35* (5), 382−388.
(55) Neurohr, G. E.; Terry, R. L.; Lengefeld, J.; Bonney, M.; Brittingham, G. P.; Moretto, F.; Miettinen, T. P.; Vaites, L. P.; Soares, L. M.; Paulo, J. A.; Harper, J. W.; Buratowski, S.; Manalis, S.; van Werven, F. J.; Holt, L. J.; Amon, A. Excessive Cell Growth Causes Cytoplasm Dilution And Contributes to Senescence. *Cell* **2019**, *176* (5), 1083−1097.e18.
(56) Guo, J.; Huang, X.; Dou, L.; Yan, M.; Shen, T.; Tang, W.; Li, J. Aging and Aging-Related Diseases: From Molecular Mechanisms to Interventions and Treatments. *Sig Transduct Target Ther* **2022**, *7* (1), 1−40.
(57) Campisi, J.; d'Adda di Fagagna, F. Cellular Senescence: When Bad Things Happen to Good Cells. *Nat. Rev. Mol. Cell Biol.* **2007**, *8* (9), 729−740.
(58) Rodier, F.; Campisi, J. Four Faces of Cellular Senescence. *J. Cell Biol.* **2011**, *192* (4), 547−556.
(59) Campisi, J. Aging, Cellular Senescence, and Cancer. *Annu. Rev. Physiol.* **2013**, *75*, 685−705.
(60) McHugh, D.; Gil, J. Senescence and Aging: Causes, Consequences, and Therapeutic Avenues. *J. Cell Biol.* **2018**, *217* (1), 65−77.
(61) Di Micco, R.; Krizhanovsky, V.; Baker, D.; d'Adda di Fagagna, F. Cellular Senescence in Ageing: From Mechanisms to Therapeutic Opportunities. *Nat. Rev. Mol. Cell Biol.* **2021**, *22* (2), 75−95.
(62) Rayess, H.; Wang, M. B.; Srivatsan, E. S. Cellular Senescence and Tumor Suppressor Gene P16. *International Journal of Cancer. Journal International du Cancer* **2012**, *130* (8), 1715.
(63) Alcorta, D. A.; Xiong, Y.; Phelps, D.; Hannon, G.; Beach, D.; Barrett, J. C. Involvement of the Cyclin-Dependent Kinase Inhibitor P16 (INK4a) in Replicative Senescence of Normal Human Fibroblasts. *Proc. Natl. Acad. Sci. U. S. A.* **1996**, *93* (24), 13742−13747.
(64) Siddiqui, M. S.; François, M.; Fenech, M. F.; Leifert, W. R. Persistent γH2AX: A Promising Molecular Marker of DNA Damage and Aging. *Mutation Research/Reviews in Mutation Research* **2015**, *766*, 1−19.
(65) Mah, L.-J.; El-Osta, A.; Karagiannis, T. C. GammaH2AX as a Molecular Marker of Aging and Disease. *Epigenetics* **2010**, *5* (2), 129−136.
(66) Aird, K. M.; Zhang, R. Detection of Senescence-Associated Heterochromatin Foci (SAHF). *Methods Mol. Biol.* **2013**, *965*, 185−196.
(67) Hernandez-Segura, A.; Nehme, J.; Demaria, M. Hallmarks of Cellular Senescence. *Trends Cell Biol.* **2018**, *28* (6), 436−453.
(68) Davies, D. M.; van den Handel, K.; Bharadwaj, S.; Lengefeld, J. Cellular Enlargement - A New Hallmark of Aging? *Frontiers in Cell and Developmental Biology* **2022**, *10*, 1036602.
(69) Lawless, C.; Wang, C.; Jurk, D.; Merz, A.; von Zglinicki, T.; Passos, J. F. Quantitative Assessment of Markers for Cell Senescence. *Experimental Gerontology* **2010**, *45* (10), 772−778.
(70) González-Gualda, E.; Baker, A. G.; Fruk, L.; Muñoz-Espín, D. A Guide to Assessing Cellular Senescence in Vitro and in Vivo. *FEBS Journal* **2021**, *288* (1), 56−80.
(71) Zhao, H.; Darzynkiewicz, Z. Biomarkers of Cell Senescence Assessed by Imaging Cytometry. *Methods Mol. Biol.* **2013**, *965*, 83−92.
(72) Paulsen, K. *Hearts Kept Ticking with Polyurethane*, February 11, 2016; ThermoFisher Scientific. https://www.thermofisher.com/blog/materials/hearts-kept-ticking-with-polyurethane/ (accessed 2023-06-27).
(73) Elfar, J.; Stanbury, S.; Menorca, R. M. G.; Reed, J. D. Composite Bone Models in Orthopaedic Surgery Research and Education. *J. Am. Acad. Orthop Surg* **2014**, *22* (2), 111−120.
(74) Park, J.-H.; Park, J.-U.; Chang, H. Advances in Biomaterials for Breast Reconstruction. *Applied Sciences* **2021**, *11* (16), 7493.
(75) Desgrandchamps, F. Biomaterials in Functional Reconstruction. *Current Opinion in Urology* **2000**, *10* (3), 201.
(76) Nicolson, P. C.; Vogt, J. Soft Contact Lens Polymers: An Evolution. *Biomaterials* **2001**, *22* (24), 3273−3283.
(77) Mastnak, T.; Maver, U.; Finšgar, M. Addressing the Needs of the Rapidly Aging Society through the Development of Multifunctional Bioactive Coatings for Orthopedic Applications. *International Journal of Molecular Sciences* **2022**, *23* (5), 2786.
(78) Chandorkar, Y.; K, R.; Basu, B. The Foreign Body Response Demystified. *ACS Biomater. Sci. Eng.* **2019**, *5* (1), 19−44.
(79) Zhang, D.; Chen, Q.; Shi, C.; Chen, M.; Ma, K.; Wan, J.; Liu, R. Dealing with the Foreign-Body Response to Implanted Biomaterials: Strategies and Applications of New Materials. *Adv. Funct. Mater.* **2021**, *31* (6), 2007226.
(80) Joukhdar, H.; Seifert, A.; Jüngst, T.; Groll, J.; Lord, M. S.; Rnjak-Kovacina, J. Ice Templating Soft Matter: Fundamental Principles and Fabrication Approaches to Tailor Pore Structure and Morphology and Their Biomedical Applications. *Adv. Mater.* **2021**, *33* (34), 2100091.
(81) Bobbert, F. S. L.; Zadpoor, A. A. Effects of Bone Substitute Architecture and Surface Properties on Cell Response, Angiogenesis, and Structure of New Bone. *J. Mater. Chem. B* **2017**, *5* (31), 6175−6192.
(82) Stevens, M. M.; George, J. H. Exploring and Engineering the Cell Surface Interface. *Science* **2005**, *310* (5751), 1135−1138.
(83) Kumar, G.; Tison, C. K.; Chatterjee, K.; Pine, P. S.; McDaniel, J. H.; Salit, M. L.; Young, M. F.; Simon, C. G. The Determination of Stem Cell Fate by 3D Scaffold Structures through the Control of Cell Shape. *Biomaterials* **2011**, *32* (35), 9188−9196.
(84) Frost, O. G.; Owji, N.; Thorogate, R.; Kyriakidis, C.; Sawadkar, P.; Mordan, N.; Knowles, J. C.; Lali, F.; Garcia-Gareta, E. Cell Morphology as a Design Parameter in the Bioengineering of Cell-Biomaterial Surface Interactions. *Biomater. Sci.* **2021**, *9* (23), 8032−8050.